Supplementary information for

On the differential expansion speeds of Indo-Pacific warm pool and deep convection favoring pool under greenhouse warming

Jeremy Cheuk-Hin Leung[1], Banglin Zhang[1,2,3]*, Qiuying Gan[1,4], Lei Wang[4], Weihong Qian[1,5], Zeng-Zhen Hu[6]

[1]Guangzhou Institute of Tropical and Marine Meteorology/Guangdong Provincial Key Laboratory of Regional Numerical Weather Prediction, CMA, Guangzhou, China

[2]College of Atmospheric Science, Lanzhou University, Lanzhou, China

[3]Southern Marine Science and Engineering Guangdong Laboratory, Zhuhai, China

[4]Laboratory for Coastal Ocean Variation and Disaster Prediction, College of Ocean and Meteorology, Guangdong Ocean University, Zhanjiang, China

[5]Department of Atmospheric and Oceanic Sciences, Peking University, Beijing, China

[6]Climate Prediction Center, NCEP/NWS/NOAA, 5830 University Research Court, College Park, MD, 20740, USA

Supplementary figures

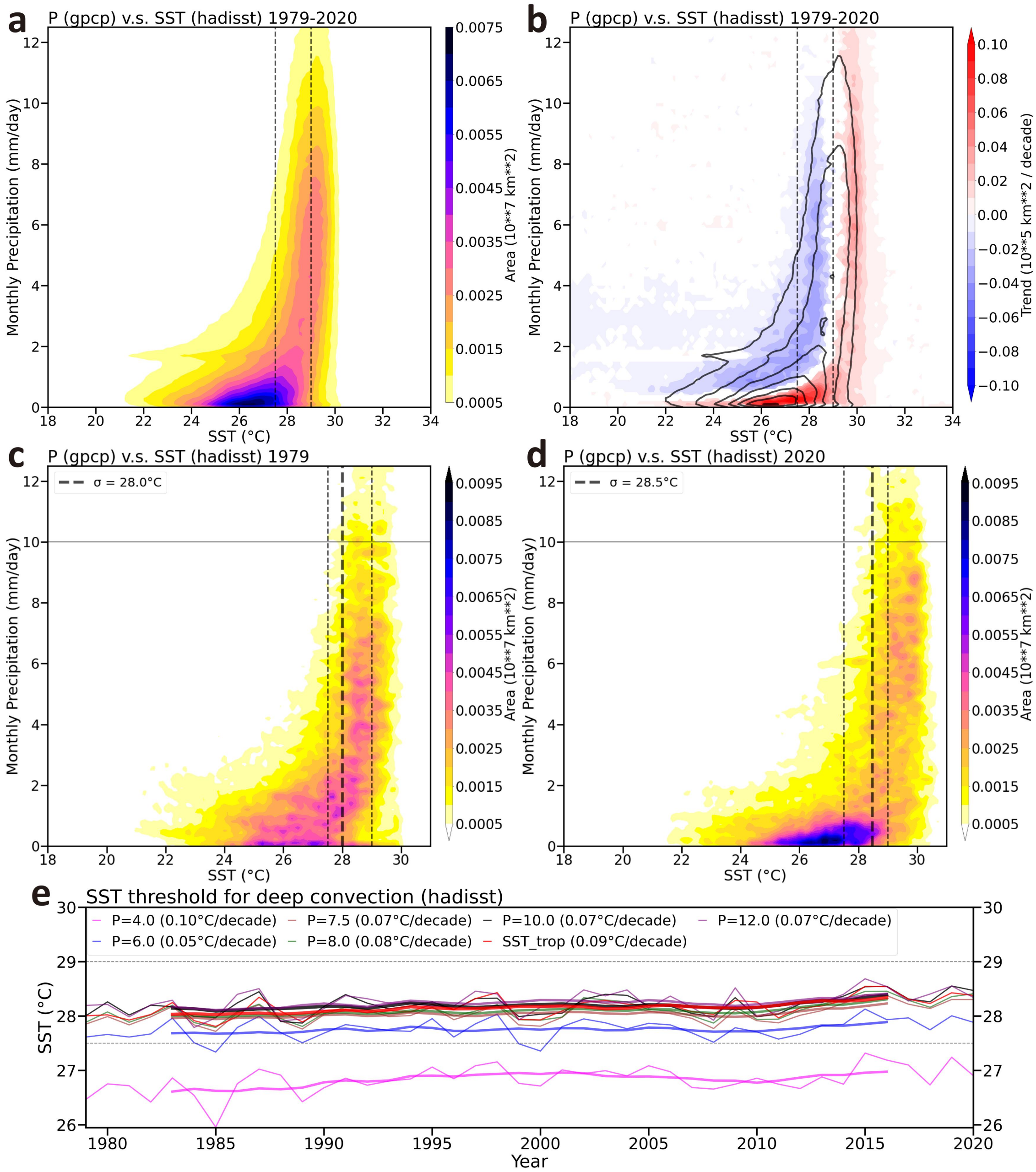

Supplementary Fig. S1: Increasing SST threshold for IPWP deep convection from 1979–2020. a–e, same as Figs. 1a–e, except that the SST data is obtained from the HadISST dataset. The linear trends of time series in (**e**) are all statistically significant at the 99.9% confidence level. The results are consistent with that shown in Fig. 1, indicating that the observed σ_{SST_conv} is not a fixed value, and has been increasing steadily since 1979.

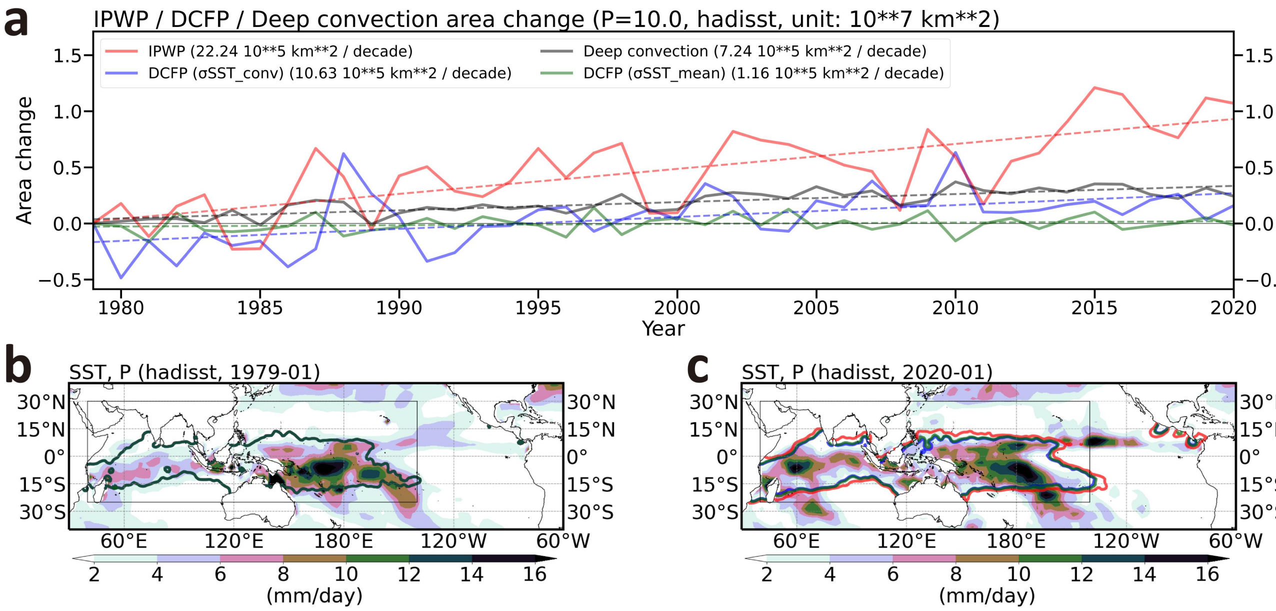

Supplementary Fig. S2: Changes in the DCFP and IPWP area in the past four decades. a–c, same as Figs. 4a–c, except that the SST data is obtained from the HadISST dataset. The red, blue, and green contours respectively indicate the regions covered by the OWP$_{SST=28}$, σ_{SST_conv}-based DCFP (σ_{SST_conv} = 28.0°C for 1979 and 28.5°C for 2020), and σ_{SST_trop}-based DCFP (σ_{SST_trop} = 28.0°C for 1979 and 28.4°C for 2020). The results are consistent with those in Fig. 4. As σ_{SST_conv} and σ_{SST_trop} increases, the traditionally defined IPWP may cover a comparatively large region without deep convection.

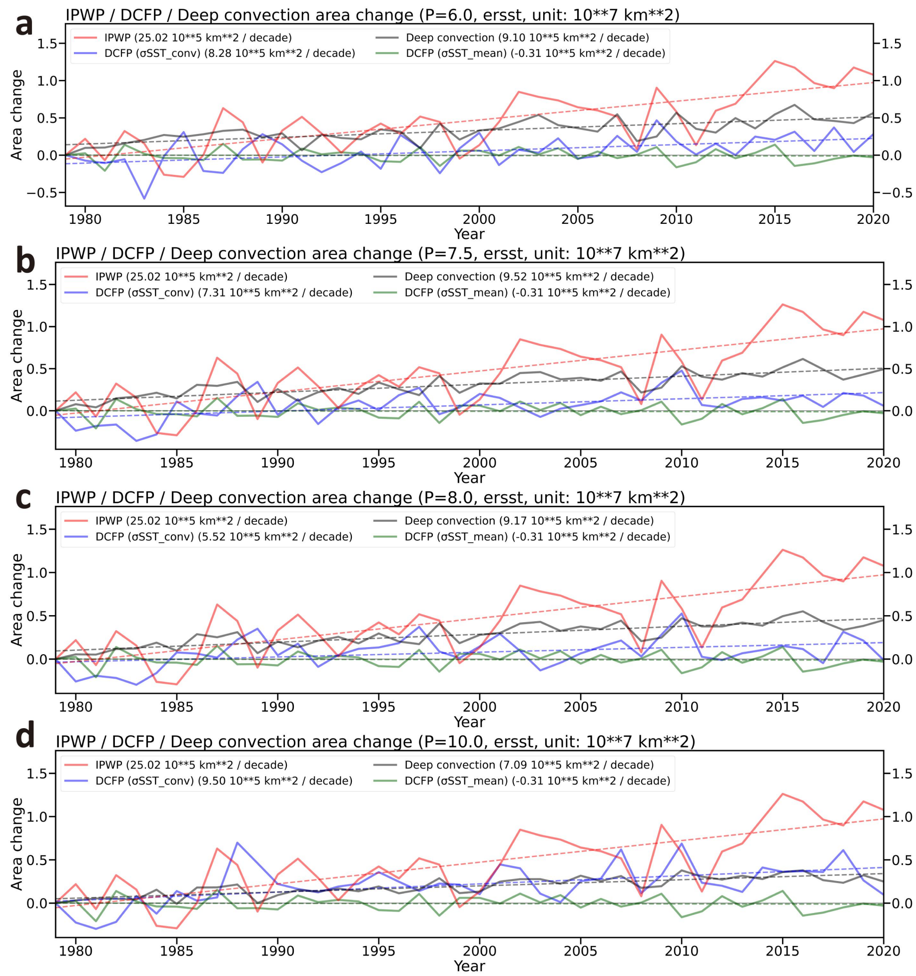

Supplementary Fig. S3: a–d, Same as Fig. 4a, except that the $DCFP_{SST\_conv}$ is defined based on different deep convection criteria: P=6.0 mm/day (**a**), P=7.5 mm/day (**b**), P=8.0 mm/day (**c**), P=10.0 mm/day (**d**), respectively. Results are based on ERSSTv5.

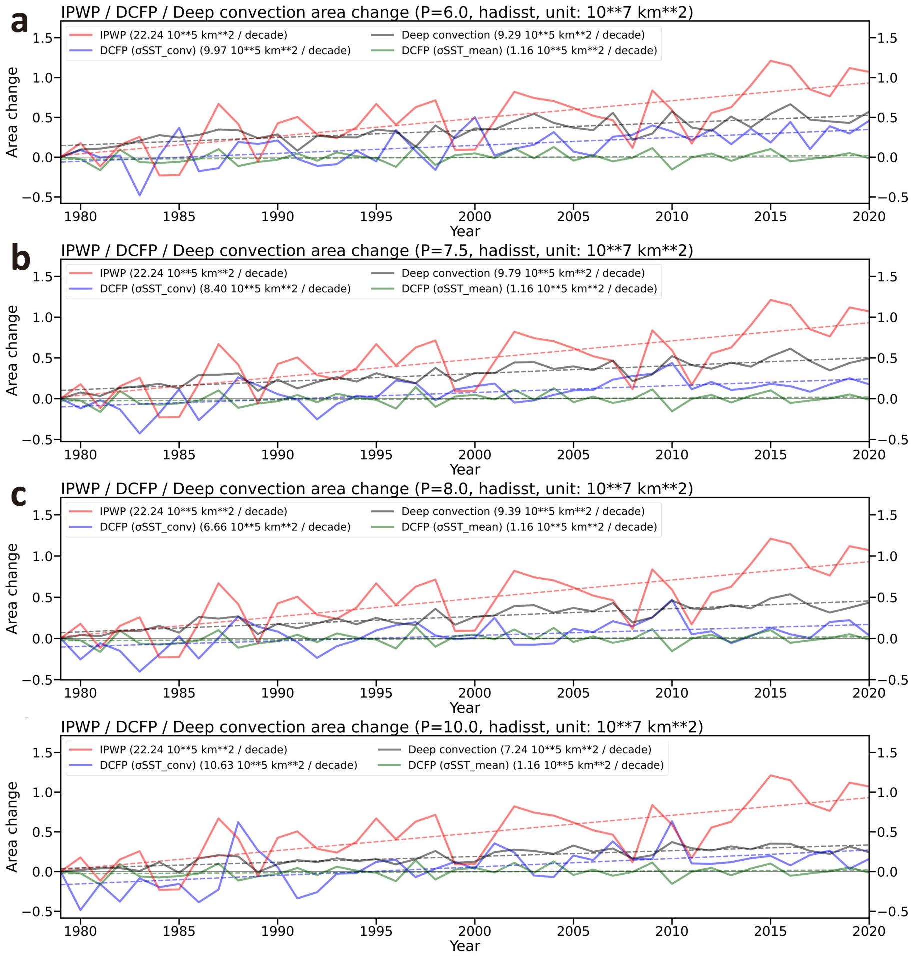

Supplementary Fig. S4: a–d, Same as Fig. 4a, except that the $DCFP_{SST\_conv}$ is defined based on different deep convection criteria: P=6.0 mm/day (**a**), P=7.5 mm/day (**b**), P=8.0 mm/day (**c**), P=10.0 mm/day (**d**), respectively. Results are based on HadISST.

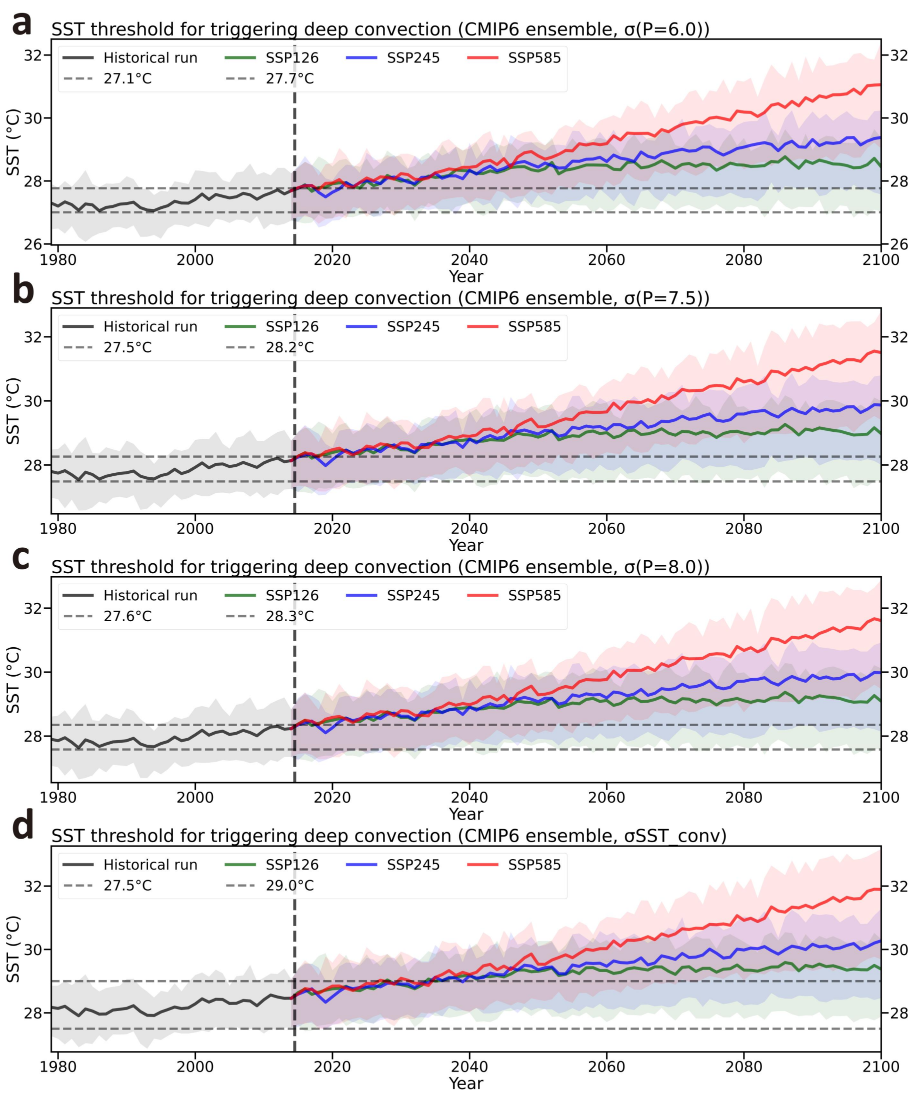

Supplementary Fig. S5: a–d, Same as Fig. 7a, except that the σ_{SST_conv} is defined based on different deep convection criteria: P=6.0 mm/day (**a**), P=7.5 mm/day (**b**), P=8.0 mm/day (**c**), P=10.0 mm/day (**d**), respectively. Results are based on the five best CMIP6 models.

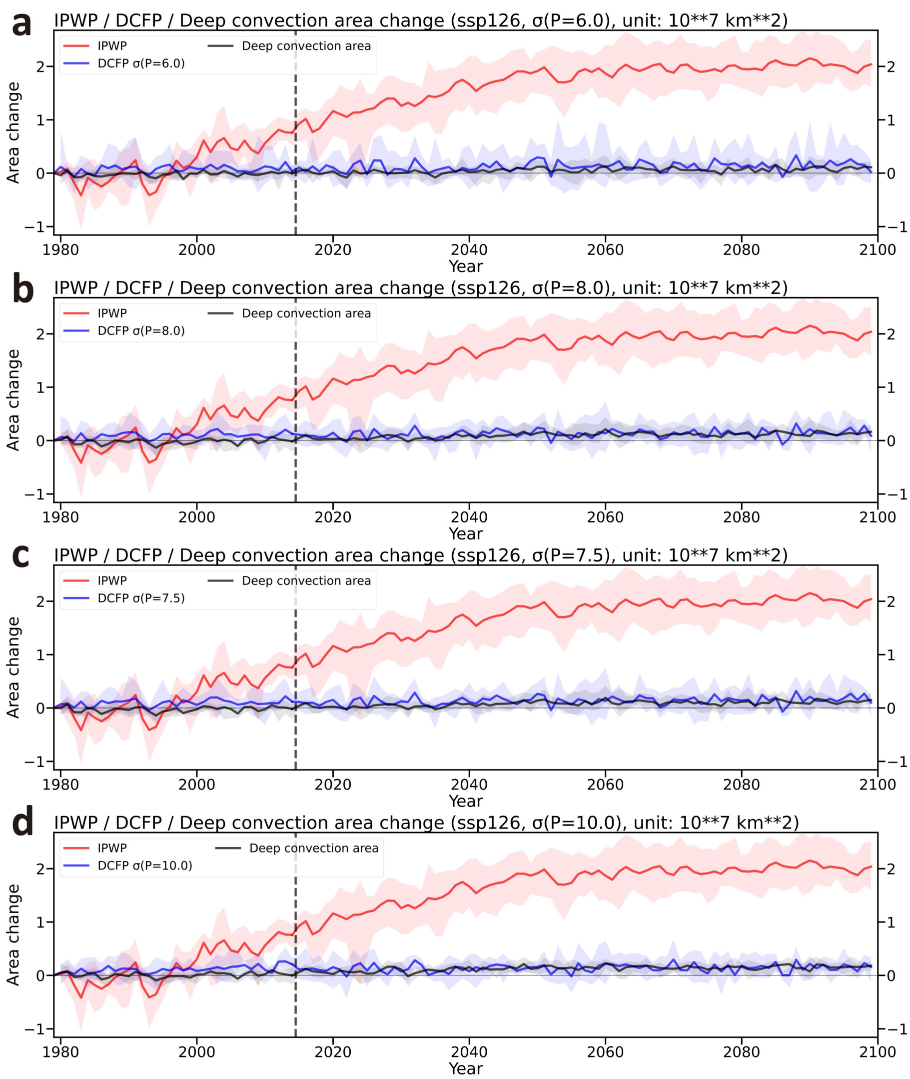

Supplementary Fig. S6: a–d, Same as Fig. 8a, except that the σ_{SST_conv} is defined based on different deep convection criteria: P=6.0 mm/day (**a**), P=7.5 mm/day (**b**), P=8.0 mm/day (**c**), P=10.0 mm/day (**d**), respectively. Results are based on the five best CMIP6 models.

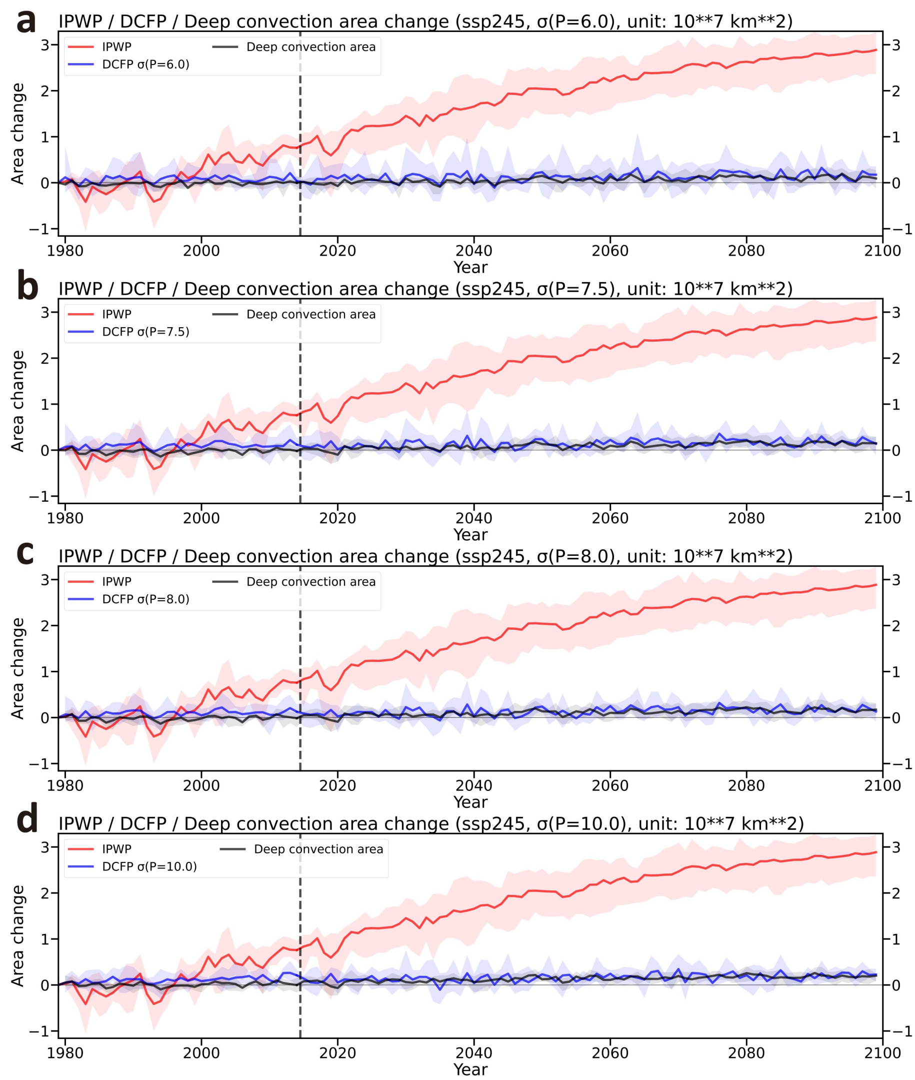

Supplementary Fig. S7: a–d, Same as Fig. 8b, except that the σ_{SST_conv} is defined based on different deep convection criteria: P=6.0 mm/day (**a**), P=7.5 mm/day (**b**), P=8.0 mm/day (**c**), P=10.0 mm/day (**d**), respectively. Results are based on the five best CMIP6 models.

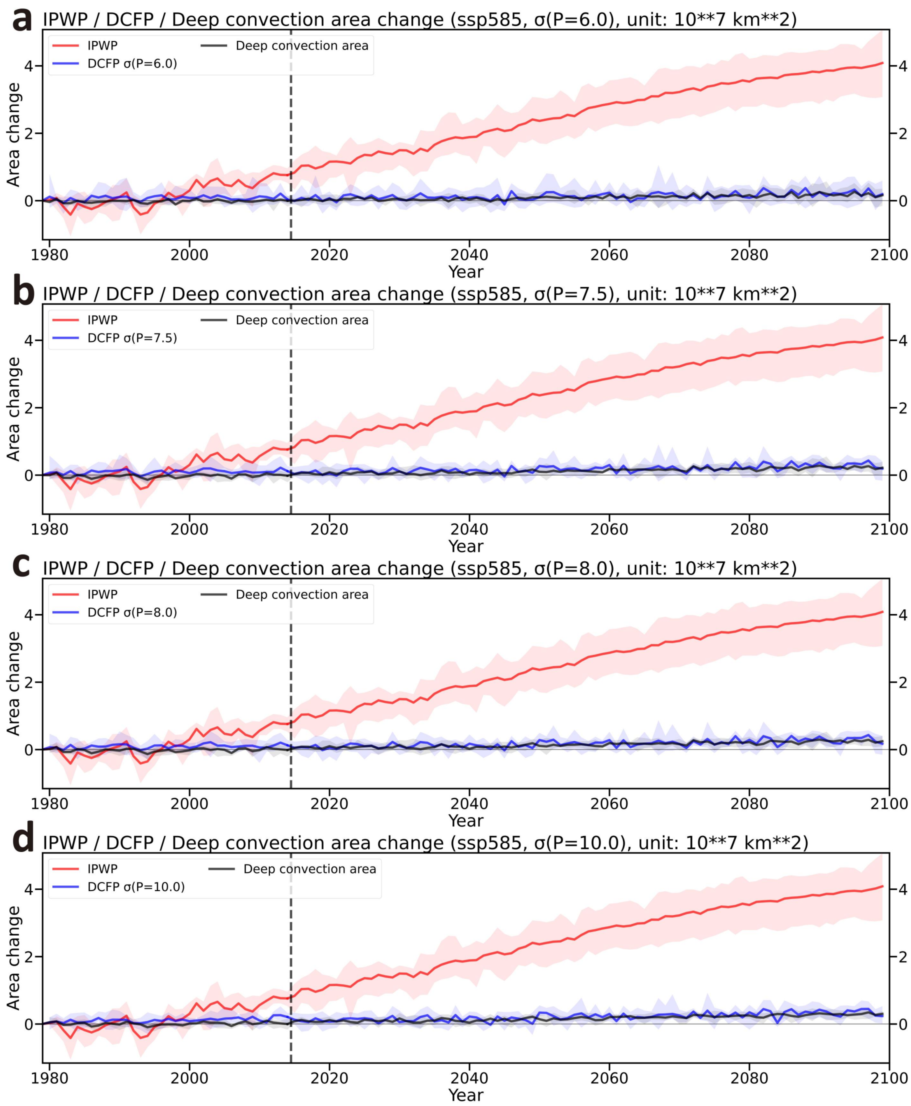

Supplementary Fig. S8: a–d, Same as Fig. 8c, except that the σ_{SST_conv} is defined based on different deep convection criteria: P=6.0 mm/day (**a**), P=7.5 mm/day (**b**), P=8.0 mm/day (**c**), P=10.0 mm/day (**d**), respectively. Results are based on the five best CMIP6 models.

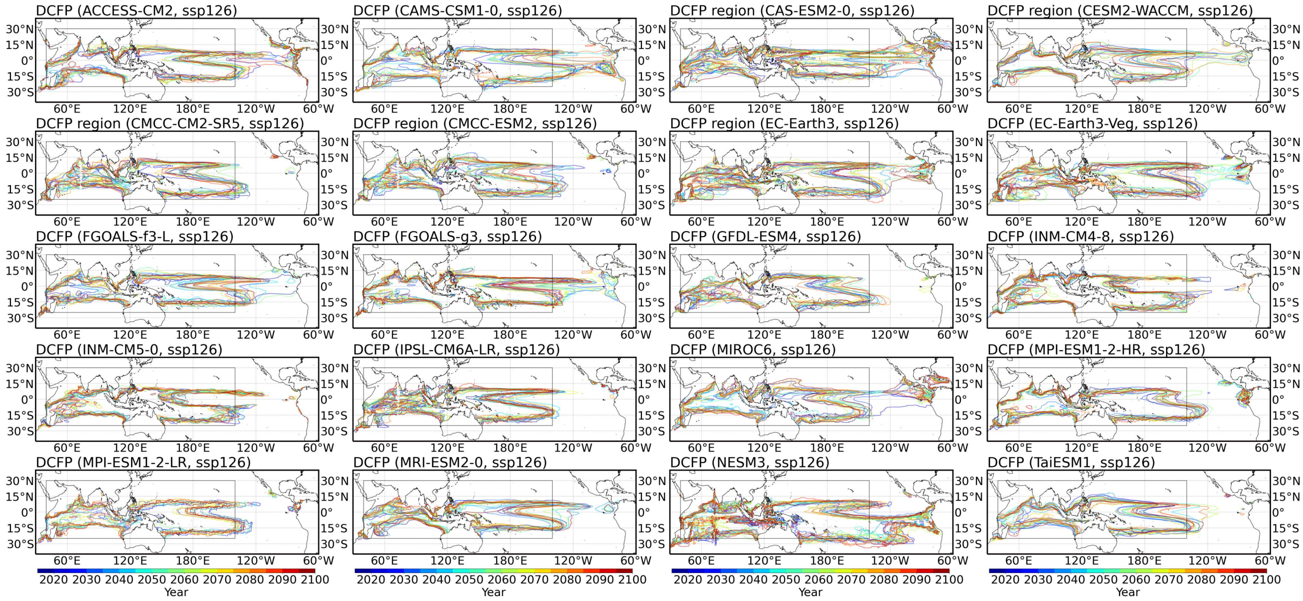

Supplementary Fig. S9: The DCFP$_{SST_conv}$ region of every 5 years from 2015–2100 under the SSP1-2.6 scenario simulated by 20 CMIP6 models.

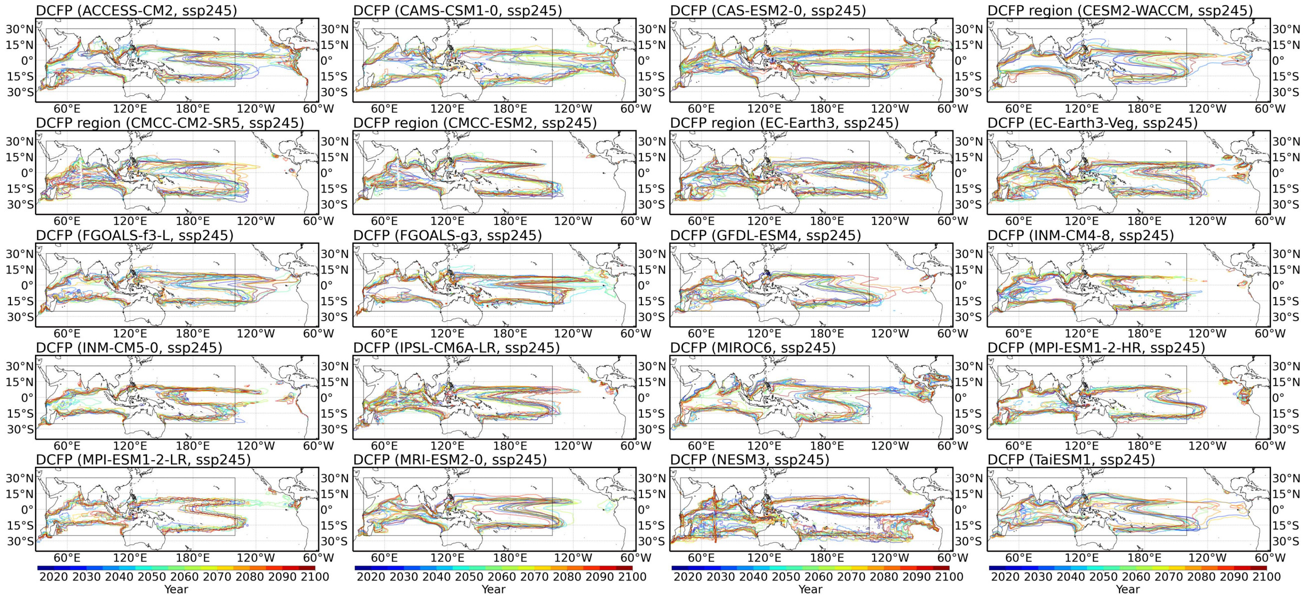

Supplementary Fig. S10: The $DCFP_{SST\_conv}$ region of every 5 years from 2015–2100 under the SSP2-4.5 scenario simulated by 20 CMIP6 models.

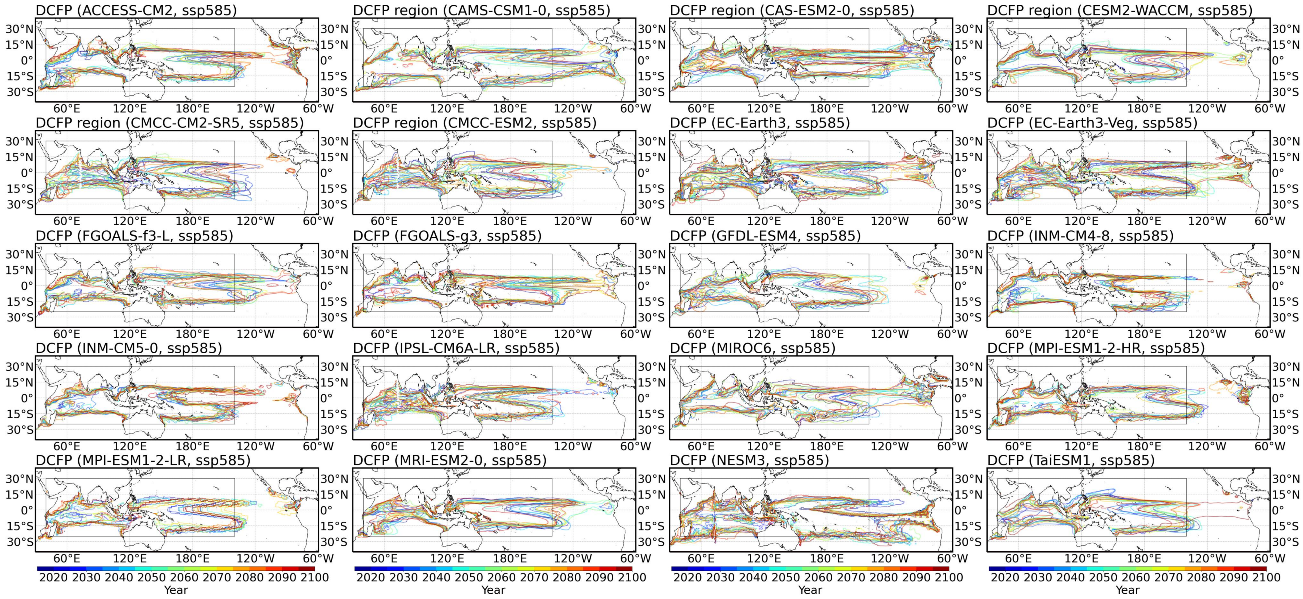

Supplementary Fig. S11: The DCFP$_{SST_conv}$ region of every 5 years from 2015–2100 under the SSP5-8.5 scenario simulated by 20 CMIP6 models.

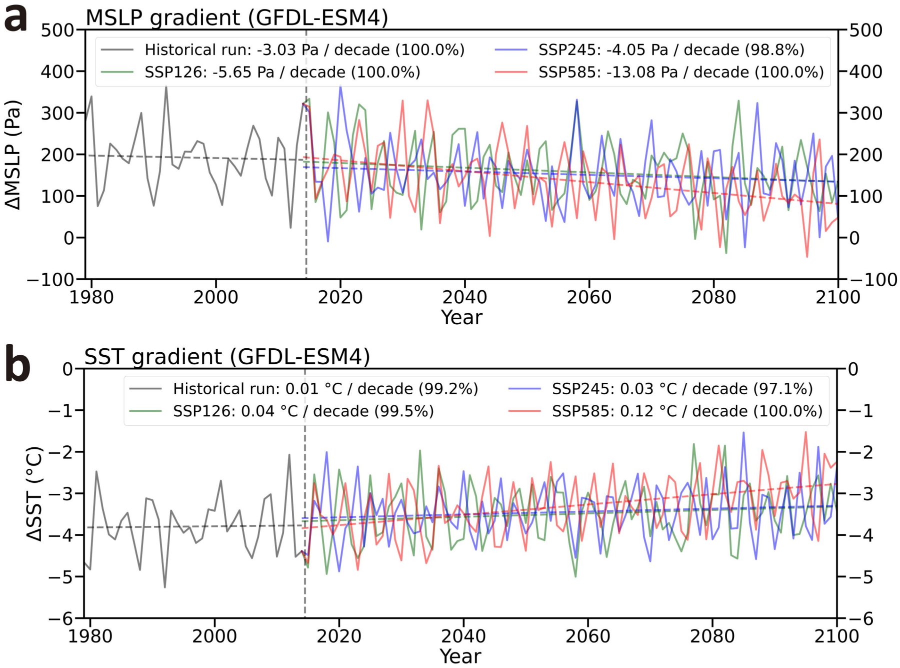

Supplementary Fig. S12: Weakening of the Pacific Walker circulation in model simulation. a, Time series of mean sea level differences (△MSLP) (units: Pa) between equatorial central/eastern Pacific (5°S–5°N, 200°–280°E) and the Indian Ocean/western Pacific (5°S–5°N, 80°–160°E), following Vecchi et al.[30], simulated by the GFDL model under the historical run (black line), SSP1-2.6 (green line), SSP2-4.5 (blue line), and SSP5-8.5 (red line), respectively**. b,** Same as (**a**), except for the SST difference (△SST) (units: °C) between equatorial central/eastern Pacific (5°S–5°N, 200°–280°E) and the Indian Ocean/western Pacific (5°S–5°N, 80°–160°E). The linear trends of all series are marked on the figure legend. Results are based on the simulation results of the GFDL model. The figure shows the weakening trends of the Pacific Walker circulation in the future climate projection under different emission scenarios.

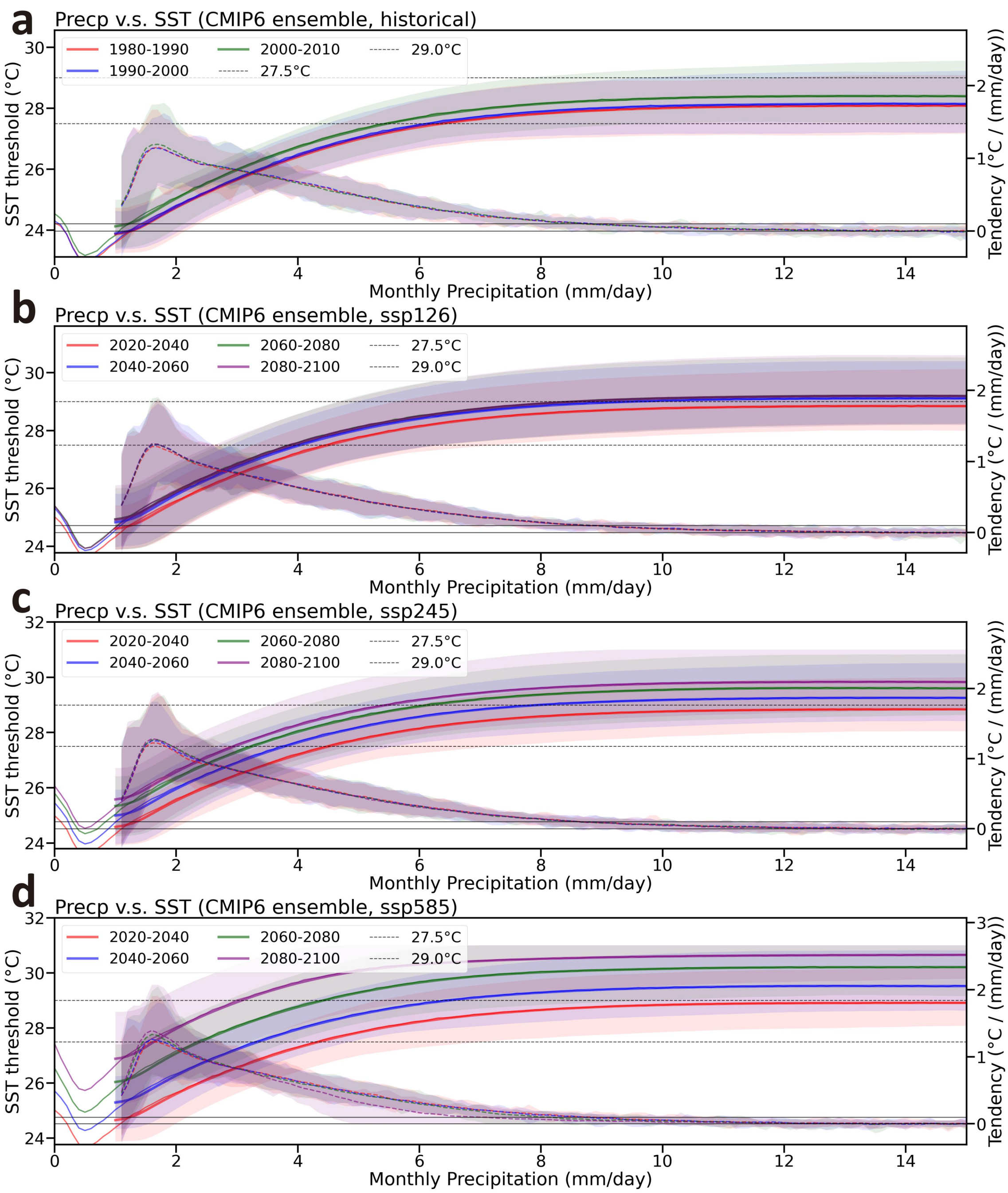

Supplementary Fig. S13: Relationship between σ_{SST_conv} and precipitation over the Indo-Pacific Ocean in future projections. a, Curve (thin solid lines) of ensemble σ_{SST_conv} (unit: °C) against precipitation (unit: mm/day) averaged over 1980–1990 (red), 1990–2000 (blue), 2000–2010 (green), based on **the historical runs of the five best CMIP6 models. b–d,** Curve (thin solid lines) of ensemble σ_{SST_conv} (unit: °C) against precipitation (unit: mm/day) averaged over 2020–2040 (red), 2040–2060 (blue), 2060–2080 (green), and 2080–2100 (green), under the **(b)** SSP1-2.6, **(c)** SSP2-4.5, and **(d)** SSP5-8.5 scenarios based on **the five best CMIP6 models**. The thick solid lines are the 21-point running mean filtered curve of the thin solid lines, which are equivalent to the 21-point running mean filtered 20% contour lines of JCFD (thick solid lines in Fig. 2). The dashed lines are the slope (first derivative, unit: °C/(mm/day)) of the 21-point running mean filtered curves. The thin horizontal black dashed lines denote 27.5°C and 29.0°C, the common range of IPWP definitions. The results show that while the σ_{SST_conv} slightly shifts upward through greenhouse warming, the relationship between σ_{SST_conv} and precipitation does not exhibit significant changes.

Table S1. Long-term trends of σ_{SST_trop} (unit: °C/decade) in the past and future projected climate change, based on ERSSTv5, HadISST, and 20 CMIP6 models. Bold texts denote the five models that could better capture the historical $DCFP_{SST\_conv}$ area trend. All trends are statistically significant at the 99.9% confidence level, except those marked with asterisks.

Observation / Models	1979–2020	1979–2014	2015–2100 (SSP1-2.6)	2015–2100 (SSP2-4.5)	2015–2100 (SSP5-8.5)
ERSSTv5	0.11	0.07	/	/	/
HadISST	0.09	0.09	/	/	/
CMIP6 Ensemble	/	0.15	0.07	0.18	0.37
CMIP6 Best	/	0.13	0.09	0.21	0.41
ACCESS-CM2	**/**	**0.14**	**0.12**	**0.23**	**0.48**
CAMS-CSM1-0	/	0.10	0.04	0.12	0.24
CAS-ESM2-0	**/**	**0.16**	**0.12**	**0.23**	**0.41**
CESM2-WACCM	**/**	**0.13**	**0.10**	**0.23**	**0.49**
CMCC-CM2-SR5	**/**	**0.10**	**0.11**	**0.22**	**0.40**
CMCC-ESM2	/	0.15	0.15	0.24	0.43
EC-Earth3	/	0.23	0.07	0.19	0.43
EC-Earth3-Veg	/	0.16	0.07	0.19	0.44
FGOALS-f3-L	/	0.17	0.03	0.14	0.32
FGOALS-g3	/	0.14	0.00*	0.11	0.27
GFDL-ESM4	/	0.16	0.04	0.13	0.31
INM-CM4-8	/	0.15	0.02	0.12	0.28
INM-CM5-0	**/**	**0.15**	**0.02**	**0.11**	**0.26**
IPSL-CM6A-LR	/	0.20	0.07	0.23	0.50
MIROC6	/	0.17	0.06	0.14	0.31
MPI-ESM1-2-HR	/	0.12	0.03	0.14	0.29
MPI-ESM1-2-LR	/	0.11	0.03	0.13	0.30
MRI-ESM2-0	/	0.09	0.07	0.18	0.36
NESM3	/	0.19	0.06	0.16	0.38
TaiESM1	/	0.17	0.15	0.26	0.45

Table S2. Long-term trends of $DCFP_{SST\_trop}$ (unit: °C/decade) in the past and future projected climate change, based on ERSSTv5, HadISST, and 20 CMIP6 models. Bold texts denote the five models that could better capture the historical $DCFP_{SST\_conv}$ area trend. All trends are statistically significant at the 99.9% confidence level, except those marked with asterisks.

Observation / Models	1979–2020	1979–2014	2015–2100 (SSP1-2.6)	2015–2100 (SSP2-4.5)	2015–2100 (SSP5-8.5)
ERSSTv5	-0.31*	0.43*	/	/	/
HadISST	1.16*	1.39*	/	/	/
CMIP6 Ensemble	/	1.44*	0.00*	0.16*	1.11
CMIP6 Best	/	3.57	0.00*	-0.37*	0.05*
ACCESS-CM2	**/**	**2.18***	**-0.17***	**-1.34***	**1.70**
CAMS-CSM1-0	/	0.87*	0.58*	-1.05*	2.35
CAS-ESM2-0	**/**	**2.83***	**-0.18***	**-0.28***	**1.32***
CESM2-WACCM	**/**	**3.73***	**-2.22**	**-2.46**	**-4.43**
CMCC-CM2-SR5	**/**	**7.94***	**2.57**	**2.36**	**1.82***
CMCC-ESM2	/	-0.05*	-0.38*	1.92*	1.69*
EC-Earth3	/	1.30*	-1.06*	0.91*	0.51*
EC-Earth3-Veg	/	1.25*	-0.40*	0.70*	1.14*
FGOALS-f3-L	/	-0.16*	0.84*	0.80*	3.79
FGOALS-g3	/	0.22*	0.84*	-0.68*	0.26*
GFDL-ESM4	/	0.39*	-0.66*	-0.33*	-0.36*
INM-CM4-8	/	-1.84*	0.00*	-1.02	-1.23
INM-CM5-0	**/**	**1.78***	**0.14***	**-0.13***	**-0.14***
IPSL-CM6A-LR	/	1.92*	0.58*	2.03	4.75
MIROC6	/	-5.43	0.67*	0.09*	-1.14*
MPI-ESM1-2-HR	/	1.92*	0.37*	0.01*	2.22
MPI-ESM1-2-LR	/	2.60*	0.65*	1.54	2.41
MRI-ESM2-0	/	2.64*	-1.16*	-0.51*	1.96
NESM3	/	1.60*	0.22*	1.11*	3.07
TaiESM1	/	3.62*	-1.57*	-0.50*	0.45*